C. R. Mecanique 344 (2016) 672–683

Contents lists available at ScienceDirect

Comptes Rendus Mecanique

www.sciencedirect.com

A lattice method for the Eulerian simulation of heavy particle suspensions

Méthode sur réseau pour la simulation eulérienne de suspensions de particules lourdes

François Laenen, Giorgio Krstulovic, Jérémie Bec *

Laboratoire Joseph-Louis-Lagrange, Université Côte d'Azur, Observatoire de la Côte d'Azur, CNRS, bd de l'Observatoire, 06300 Nice, France

ARTICLE INFO

Article history:
Received 11 March 2016
Accepted 24 May 2016
Available online 10 June 2016

Keywords:
Disperse flows
Particles in turbulence
Eulerian modeling
Lattice methods

Mots-clés :
Écoulements dispersés
Particules en turbulence
Modélisation eulérienne
Méthodes sur réseau

ABSTRACT

Modeling dispersed solid phases in fluids still represents a computational challenge when considering a small-scale coupling in wide systems, such as the atmosphere or industrial processes at high Reynolds numbers. A numerical method is here introduced for simulating the dynamics of diffusive heavy inertial particles in turbulent flows. The approach is based on the position/velocity phase–space particle distribution. The discretization of velocities is inspired from lattice Boltzmann methods and is chosen to match discrete displacements between two time steps. For each spatial position, the time evolution of particles momentum is approximated by a finite-volume approach. The proposed method is tested for particles experiencing a Stokes viscous drag with a prescribed fluid velocity field in one dimension using a random flow, and in two dimensions with the solution to the forced incompressible Navier–Stokes equations. Results show good agreements between Lagrangian and Eulerian dynamics for both spatial clustering and the dispersion in particle velocities. In particular, the proposed method, in contrast to hydrodynamical Eulerian descriptions of the dispersed phase, is able to reproduce fine particle kinetic phenomena, such as caustic formation or trajectory crossings. This indicates the suitability of this approach at large Stokes numbers for situations where details of collision processes are important.

RÉSUMÉ

La modélisation de particules solides dispersées dans un fluide reste actuellement un défi numérique, surtout lorsqu'il y a une grande séparation d'échelles entre le couplage et l'écoulement, comme par exemple dans l'atmosphère ou les écoulements industriels à grand nombre de Reynolds. Une méthode numérique est ici présentée dans le but de simuler la dynamique de particules lourdes diffusives dans des écoulements turbulents. L'approche est basée sur la distribution des particules dans l'espace des phases positions–vitesses. La discrétisation en vitesses s'inspire de la méthode de Boltzmann sur réseau et est choisie de telle manière à ce qu'elle corresponde à des déplacements discrets entre deux pas de temps. Pour chaque position spatiale, l'évolution temporelle de la quantité

* Corresponding author.
E-mail addresses: francois.laenen@oca.eu (F. Laenen), giorgio.krstulovic@oca.eu (G. Krstulovic), jeremie.bec@oca.eu (J. Bec).

http://dx.doi.org/10.1016/j.crme.2016.05.004
1631-0721/

de mouvement est résolue par une approche de volumes finis. La méthode proposée est testée pour des particules soumises à un frottement visqueux de Stokes, avec des écoulements aléatoires en une dimension, et avec des solutions de l'équation de Navier–Stokes incompressible forcée en deux dimensions. Les résultats montrent un bon accord entre les simulations lagrangiennes et eulériennes pour reproduire les concentrations préférentielles et la dispersion des vitesses des particules. De plus, la méthode proposée, contrairement à des descriptions hydrodynamiques des suspensions, permet de résoudre le croisement de trajectoires et la formation de caustiques, ce qui montre sa pertinence aux grands nombres de Stokes pour les situations où les détails des processus de collision sont importants.

1. Introduction

Particle-laden turbulent flows are found in numerous natural and industrial situations, ranging from droplet growth in clouds and dust accretion in early stellar systems, to turbulent mixing in engines and industrial sprays. In such situations, the processes that need being modeled and quantified involve the fine-scale dynamical properties of the particles, like preferential concentration, collisions and coalescences, chemical reactions, and modulation of the fluid flow by the particles. To address specific microphysical issues, one usually study simultaneously the turbulent flow and the dispersed phase using Eulerian–Lagrangian direct numerical simulations (see, for instance [1,2], for recent reviews). This approach is particularly suited for monitoring the fluctuations occurring at dissipative scales. However, direct numerical simulations are quickly too computationally expensive for studying particle suspensions in realistic settings. On the one hand, a large-scale system, such as a chemical reactor, an atmospheric cloud or a protoplanetary disk, contains a prohibitively large number of particles. On the other hand, the substantial Reynolds numbers of natural and industrial flows require the use of large-scale models, such as large-eddy simulations. Eulerian–Lagrangian methods, where the dispersed phase is approached by point particles, show some advantages: they allow for an easy implementation of polydispersity and are rather insensitive to subgrid-scale fluctuations, at least for particles with a large-enough response time [3]. For particles with smaller inertia, one relies on the use of stochastic Langevin models [4,5]. In addition the constraints on the number of particles can be relaxed using super-particles approaches, which then necessitates some modeling for collisions [6,7]. However, as stressed for instance in [8], Lagrangian methods prove some difficulties in correctly predicting modifications of the carrier flow by the dispersed phase, particle-to-particle interactions and near-wall effects.

Some of these shortcomings can be circumvent using Eulerian–Eulerian methods (see [9] for a review). The main difficulty then relies in finding a fluid description of the dispersed particulate phase. In principle, this is achieved by prescribing a closure for the kinetic hierarchy of moment equations. When considering an ensemble of particle trajectories $(\boldsymbol{x}_\mathrm{p}, \boldsymbol{v}_\mathrm{p})$, one naturally introduces the phase–space density

$$f(\boldsymbol{x}, \boldsymbol{v}, t) = \left\langle \delta(\boldsymbol{x}_\mathrm{p}(t) - \boldsymbol{x})\, \delta(\boldsymbol{v}_\mathrm{p}(t) - \boldsymbol{v}) \right\rangle \tag{1}$$

where the fluid velocity realization is fixed and the average $\langle\cdot\rangle$ is both over the particle ensemble (different realizations of the initial conditions for particle positions and velocities and/or average over a large number of particles) and over the molecular diffusion of the particles (with diffusion constant κ). Let us stress again that this average is not over the fluid velocity fluctuations, so that the density f is not a probability density function but rather the instantaneous phase–space density of particles. It solves the diffusion-transport equation

$$\partial_t f + \boldsymbol{v} \cdot \nabla_{\boldsymbol{x}} f + \nabla_{\boldsymbol{v}} \cdot \left[f\, \mathcal{F}(\boldsymbol{x}, \boldsymbol{v}, t)/m_\mathrm{p} \right] - \nabla_{\boldsymbol{v}} \cdot (\kappa \nabla_{\boldsymbol{v}} f) = 0 \tag{2}$$

where $\mathcal{F}$ is the force exerted by the fluid on a particle located at $\boldsymbol{x}$ with a velocity $\boldsymbol{v}$ and m_p is the particle mass. This Liouville equation relates to the continuity of the particle distribution in the phase space and is exact. It describes the full dynamics of small particles, the drift terms are completely prescribed by a given realization of the fluid flow, so that equation (2) is not a closure. It is actually equivalent to the kinetic formulation of plasma dynamics or gravitational gases for which the phase–space density solves a Vlasov equation. Our approach is thus different from PDF closures developed for instance in [10–12].

To obtain an Eulerian description of particles dynamics that depends on the spatial variable $\boldsymbol{x}$ only, the usual approach consists in deriving the equations for the various moments of the velocity $\boldsymbol{v}$. To close the resulting hierarchy, additional assumptions are needed. They naturally arise when focusing on given asymptotics (see, e.g., [13]). For instance, when the particles experience a very strong viscous drag with the flow (small Stokes numbers), an effective particle velocity can be written [14] leading to close this hierarchy at the zeroth order and to write an explicit equation for the transport of particle density. This then serves as a basis for deriving subgrid-scale models for large-eddy simulations (see, e.g., [15]). First-order closures lead to writing an evolution equation for a particle velocity field that is coupled to the fluid flow. Again, such methods are limited to asymptotically small values of the Stokes number, as they are inadequate to deal with

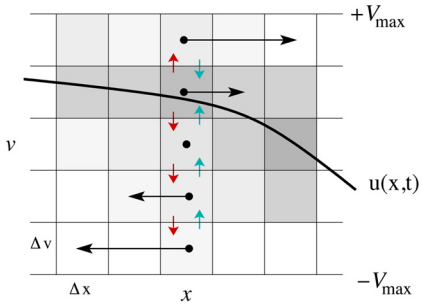

Fig. 1. Sketch of the lattice dynamics in the (x, v) position–velocity phase space. The solid curve is the fluid velocity profile; the grey scale tiling represents the discretization of particles mass in phase space. The black horizontal arrows show advection, while the blue and red vertical arrows are forcing and diffusion, respectively.

multi-streamed particle distributions. It is indeed well known that the trajectories of finite-Stokes-number particles can cross, leading to the formation of regions where the particle velocities are multivalued and cannot be described in terms of a spatial field. This phenomenon is usually referred to as *particle-trajectory crossing* [16], *sling effect* [17] or *caustic formation* [18], and has important impacts in estimating collision rates (see, e.g., [19]). Higher-order closures, such as ten-moment equations, can also be proposed depending on the specific forces applied on the particles. They account for the dispersion in particle velocities and can thus catch some aspects of multi-streaming (using either algebraic or quadrature closures [20,21]).

In principle, accessing the full multi-streaming dynamics of particles requires solving the kinetic equation (2) in the entire $(2 \times d)$-dimensional position–velocity phase space. (d denotes here the dimension of the physical space.) A clear difficulty which is then faced is the prohibitive computational cost of integrating a partial differential equation in a space with such a large dimensionality. Attempts have nevertheless been made by decreasing the number of relevant degrees of freedom. This can be easily done, for instance, by considering one-dimensional flows [13]. Other approaches are based on the physical observation that the distribution of particle velocities is usually rather concentrated along a given number of branches in phase space. This led for instance to capture implicitly the velocity dispersion by applying a level-set method in phase space [22]. The efficient implementation of this procedure to high-dimensional turbulent situations still represents a real challenge.

Here, we propose an alternative approach that consists in degrading the resolution in velocities and to apply computationally efficient ideas inspired from lattice Boltzmann methods [23]. The discrete values of velocities are chosen to correspond exactly to discrete displacements between two time steps on a fixed spatial lattice. The time evolution of $f(\boldsymbol{x}, \boldsymbol{v}, t)$ is then approximated by splitting the spatial advection on the lattice and the acceleration of particles, which is integrated using a finite-volume scheme. This gives access to a full phase–space particle distribution that naturally catch multi-streaming. This method is relevant to cases where diffusion is responsible for a broadening of the particle velocity dispersion and it applies to any kind of force $\mathcal{F}$ acting on the particles. After describing the algorithm in Sec. 2, we present some qualitative and quantitative tests for very small heavy particles whose dynamics is dominated by diffusion and a Stokes drag with the fluid velocity. The proposed lattice–particle method is directly compared to the results of direct Lagrangian simulations. Section 3 is devoted to the one-dimensional case with a random Gaussian flow. Section 4 shows the results of coupled Navier–Stokes and lattice particles simulations in two dimensions for turbulent flows, in the inverse cascade of kinetic energy.

2. Description of the method

The solutions $f(\boldsymbol{x}, \boldsymbol{v}, t)$ to the Liouville equation (2) are defined in the full position–velocity phase–space $\Omega \times \mathbb{R}^d$, where Ω designates a d-dimensional bounded spatial domain. To simulate numerically the dynamics, we divide the phase–space in $(2 \times d)$-dimensional hypercubes. We then approximate $f(\boldsymbol{x}, \boldsymbol{v}, t)$ as a piecewise-constant scalar field on this lattice. Positions are discretized on a uniform grid with spacing Δx in all directions. In principle, f has to be defined for arbitrary large velocities. We however assume that relevant values of $\boldsymbol{v}$ are restricted to a bounded interval $[-V_{\max}, V_{\max}]^d$, where $V_{\max}$ has to be specified from physical arguments based on the forces $\mathcal{F}$ applied on the particles. Velocities are assumed to take N_v^d values, so that the grid spacing reads $\Delta v = 2\,V_{\max}/N_v$. Fig. 1 illustrates the phase–space discretization in the one-dimensional case with $N_v = 5$. The various cells in position–velocity contain a given mass of particles. All these particles are assumed to have a position and velocity equal to that at the center of the cell.

The three phase–space differential operators appearing in Eq. (2), namely the advection, the particle forcing, and the diffusion, are applied one after the other, following an *operator splitting* method [24]. For the advection step, we use a technique inspired from the lattice Boltzmann method (see [25]). The time stepping is chosen, so that a discrete velocity exactly matches a shift in positions by an integer number of gridpoints. Namely, we prescribe $\Delta x = \Delta v\,\Delta t$. All the particle phase–space mass located in $[-\Delta v/2, \Delta v/2]$ does not move; that in $[\Delta v/2, 3\Delta v/2]$ is shifted by one spatial gridpoint to the right and that in $[-3\Delta v/2, -\Delta v/2]$ to the left, etc. All the mass is displaced from one cell to another according to its

own discrete velocity value. This evolution is sketched by black horizontal arrows in Fig. 1. This specific choice for the time-stepping implies that the advection (in space) is treated exactly for the discrete system. The next steps consist in applying the force acting on the particles and the diffusion. The corresponding terms in Eq. (2) are conservation laws, which suggests using a finite-volume approximation. The time evolutions due to forcing and diffusion are performed successively. In both cases, we use classical schemes (see below), where zero-flux conditions are imposed on the boundary of $[-V_{\max}, V_{\max}]^d$. The force is evaluated using the values of $\boldsymbol{v}$ at the centers of the cells and $\nabla_v f$ is approximated using finite differences. These steps are illustrated by the horizontal blue and red arrows in Fig. 1.

A few comments on the convergence and stability of the proposed method. Clearly, except for specific singular forcings, all the linear differential operators involved in (2) are expected to be bounded.[1] We can thus invoke the equivalence (or Lax–Richtmyer) theorem for linear differential equations that ensures convergence, provided the scheme is stable and consistent [24].

For the operator associated with particle acceleration, we use in this study either a first-order upwind finite-volume scheme or a higher-order flux limiter by following the strategy proposed in [26]. The upwind scheme is first-order accurate and is wellknown for being consistent and stable if it satisfies the Courant–Friedrichs–Lewy (CFL) condition. This requires that the time needed to accelerate particles by the grid size Δv is larger than the time step Δt, leading to the stability condition

$$\mathrm{CFL} = (\Delta t/\Delta v) \max_{\boldsymbol{x},\boldsymbol{v},t} |\mathcal{F}(\boldsymbol{x}, \boldsymbol{v}, t)|/m_{\mathrm{p}} < 1 \tag{3}$$

The upwind scheme is however known to suffer from numerical diffusion, and obviously, one should only expect to recover the correct dynamics only when the numerical diffusion κ_{num} is much smaller than the physical one κ. The average numerical diffusion can be estimated as $\langle \kappa_{\mathrm{num}} \rangle \approx \langle \mathcal{F} \rangle \Delta t/\Delta v$. To limit the effects of this numerical diffusion, we have also used a flux-limiter scheme. While taking benefit of a higher-order approximation where the field is smooth, it uses the ratio between consecutive flux gradients to reduce the order in the presence of strong gradients only. The limiter is a nonlinear function of the phase–space density field and the stability is ensured provided that it is total-variation diminishing (TVD), see [24]. Among the various available TVD limiters, we choose the scheme proposed in [27] with parameter 2/3.

For the term associated with diffusion, the flux at the interface between two velocity cells is computed using finite differences. The resulting finite-volume scheme is thus equivalent to compute a discrete Laplacian on the velocity mesh. The stability condition is then given by

$$\frac{\kappa \Delta t}{\Delta v^2} < \frac{1}{2} \tag{4}$$

To summarize, the stability and convergence of the proposed method is ensured when both (3) and (4) are satisfied.

From now on we restrict ourselves to small and heavy particles whose interaction with the carrier fluid is dominated by viscous drag and diffusion. In that case, we have

$$\frac{\mathrm{d}\boldsymbol{v}_{\mathrm{p}}}{\mathrm{d}t} = -\frac{1}{\tau_{\mathrm{p}}} \left(\boldsymbol{v}_{\mathrm{p}} - \boldsymbol{u}(\boldsymbol{x}_{\mathrm{p}}, t) \right) + \sqrt{2\kappa}\, \boldsymbol{\eta}(t) \tag{5}$$

where $\boldsymbol{\eta}(t)$ is the standard d-dimensional white noise and the fluid velocity field $\boldsymbol{u}(\boldsymbol{x}, t)$ is prescribed and assumed to be in a (statistically) stationary state. This Stokes drag involves the viscous particle response time $\tau_{\mathrm{p}} = 2\rho_{\mathrm{p}} a^2/(9\rho_{\mathrm{f}}\nu)$, with a the radius of the particles, ν the viscosity of the fluid, $\rho_{\mathrm{p}} \gg \rho_{\mathrm{f}}$ the particle and fluid mass densities, respectively. Inertia is quantified by the Stokes number $St = \tau_{\mathrm{p}}/\tau_{\mathrm{f}}$, where τ_{f} is a characteristic time of the carrier flow. The diffusion results from the random collisions between the considered macroscopic particle and the molecules of the underlying gas. Assuming thermodynamic equilibrium, the diffusion coefficient reads $\kappa = 2k_{\mathrm{B}}T/(m_{\mathrm{p}}\tau_{\mathrm{p}})$, where k_{B} is the Boltzmann constant and T the absolute temperature. The effect of diffusion is measured by the non-dimensional number $\mathcal{K} = \kappa\, \tau_{\mathrm{f}}/U_{\mathrm{f}}^2$ (U_{f} being a characteristic velocity of the fluid flow).

Such a specific dynamics leads to appropriate estimates for the bound $V_{\max}$ in particle velocity. One can indeed easily check that when $\kappa = 0$, we always have $|\boldsymbol{v}_{\mathrm{p}}| \leq \max_{\boldsymbol{x},t} |\boldsymbol{u}(\boldsymbol{x}, t)|$. In a deterministic fluid flow, as for instance when $\boldsymbol{u}$ is stationary, this gives the natural choice $V_{\max} = \max_{\boldsymbol{x},t} |\boldsymbol{u}(\boldsymbol{x}, t)|$. However, in most situations, the maximal fluid velocity is not known a priori. One then relies on the statistical properties of $\boldsymbol{u}$, as for instance its root-mean square value $u_{\mathrm{rms}} = \langle u_i^2 \rangle^{1/2}$. Usually the one-time, one-point statistics of fluctuating velocity fields (being random or turbulent) are well described by a Gaussian distribution. This ensures that by choosing $V_{\max} = 3\, u_{\mathrm{rms}}$, the probability that a particle has a velocity out of the prescribed bounds is less than 1%. Such estimates are rather rough. In practice, it is known that the typical particle velocity decreases as a function of the Stokes number. It was for instance shown in [28] that $\langle |\boldsymbol{v}_{\mathrm{p}}|^2 \rangle \propto u_{\mathrm{rms}}^2/St$ at very large Stokes numbers. An efficient choice for $V_{\max}$ should account for that.

In the next two sections we investigate two different cases: First a one-dimensional random Gaussian carrier flow with a prescribed correlation time and, second, a two-dimensional turbulent carrier flow that is a solution to the forced incompressible Navier–Stokes equation.

[1] Notice that, although the velocity might explicitly appear in the force $\mathcal{F}$, we only solve for a compact domain of velocities, thus preventing divergences.

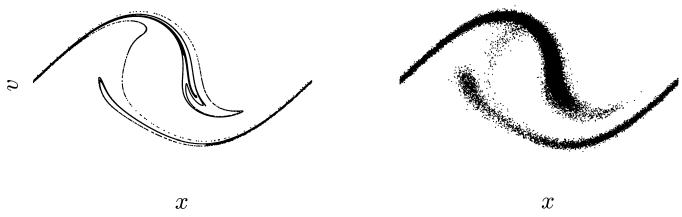

Fig. 2. Instantaneous snapshots of the particle positions in the (x, v) plane for $St \approx 2$ and with no diffusion ($\mathcal{K} = 0$, Left) and with diffusion ($\mathcal{K} = 6 \times 10^{-4}$, Right). The folded structures are spread out by diffusion.

3. Application to a one-dimensional random flow

3.1. Particle dynamics for $d = 1$

In this section, we test our method in a one-dimensional situation. For that, we assume that the fluid velocity is a Gaussian random field, which consists in the superposition of two modes whose amplitudes are Ornstein–Uhlenbeck processes, namely

$$u(x,t) = A_1(t)\cos(2\pi x/L) + A_2(t)\sin(2\pi x/L) \tag{6}$$

$$\frac{\mathrm{d}A_i(t)}{\mathrm{d}t} = -\frac{1}{\tau_\mathrm{f}}A_i(t) + \sqrt{\frac{2}{\tau_\mathrm{f}}}\,\xi_i(t) \tag{7}$$

where the ξ_i's are independent white noises with correlations $\langle \xi_i(t)\,\xi_i(t')\rangle = u_{\mathrm{rms}}^2\,\delta(t-t')$. This flow is by definition fully compressible (potential) and spatially periodic with period L. It is characterized by its amplitude $\langle (u(x,t))^2\rangle^{1/2} = u_{\mathrm{rms}}$ and its correlation time τ_f, which are fixed parameters. We focus on the case when the Kubo number $Ku = \tau_\mathrm{f}\,u_{\mathrm{rms}}/L$ is of the order of unity.

We next consider particles suspended in this flow and following the dynamics (5). The relevant Stokes number is then defined as $St = \tau_\mathrm{p}\,u_{\mathrm{rms}}/L$ and the relative impact of diffusion is measured by $\mathcal{K} = \kappa L/u_{\mathrm{rms}}^3$. When diffusion is neglected ($\mathcal{K} \to 0$), the particles distribute on a dynamical attractor (see Fig. 2, Left) whose properties depend strongly on St. These strange attractors are typically fractal objects in the phase space and they are characterized by their fractal dimension spectrum [29]. The locations of particles are obtained by projecting theses sets on the position space and might thus inherit the associated clustering [30]. The dimension that is relevant for binary interactions between particles is the correlation dimension $\mathcal{D}_2$, which relates to the probability of having two particles within a given distance, namely

$$p_2^<(r) = \mathbb{P}(|\boldsymbol{x}_\mathrm{p}^{(1)}(t) - \boldsymbol{x}_\mathrm{p}^{(2)}(t)| < r) \sim (r/L)^{\mathcal{D}_2},\ \text{for } r \ll L \tag{8}$$

where $\boldsymbol{x}_\mathrm{p}^{(1)}$ and $\boldsymbol{x}_\mathrm{p}^{(2)}$ denote the positions of two different particles. Note that as we consider u to be in a statistically stationary state, $p_2^<$ is independent of time. The correlation dimension $\mathcal{D}_2$ varies from $\mathcal{D}_2 = 0$ for a point concentrations to $\mathcal{D}_2 = 1$ for a homogeneous mass distribution. In the example of Fig. 2 (Left) $\mathcal{D}_2 \approx 0.7$. The variations of $\mathcal{D}_2$ as a function of the Stokes number are displayed in the inset of Fig. 3. $\mathcal{D}_2$ indeed varies from 0 at small Stokes numbers to values close to one. For $St = 0$, the particles concentrate on a point; their distribution is said to be atomic and $\mathcal{D}_2 = 0$. This is a consequence of the compressibility of the one-dimensional (potential) flow. Actually this behavior persists for finite Stokes numbers, up to a critical value $St^\star$, as shown in [31] in the case where $\tau_\mathrm{f} \ll L/u_{\mathrm{rms}}$ (that is $Ku \to 0$). We observe here $St^\star \approx 0.6$. For $St > St^\star$, the dimension increases and tends to a homogeneous distribution ($\mathcal{D}_2 = 1$) at large particle inertia.

When one has only access to the Eulerian density of particles, the distribution of distances cannot be directly inferred from (8). One then relies on the coarse-grained density of particles

$$\rho_r(x,t) = \int_{-r/2}^{r/2} \mathrm{d}x' \int \mathrm{d}v\ f(x+x', v, t) \tag{9}$$

It is known that, under some assumptions on the ergodicity of the particle dynamics, the second-order moment of this quantity scales as $\langle \rho_r^2\rangle \propto r^{\mathcal{D}_2 - 1}$ (see, e.g., [29]). In one dimension, this second-order moment is exactly the same as the radial distribution function. This quantity will be used in the next sections to address the physical relevance of the lattice–particle method. It is of particular interest when considering collisions between particles. Indeed, as explained for instance in [32], the ghost-collision approximation leads to write the collision rate between particles as the product of two contributions: one coming from clustering and entailed in the radial distribution function, and another related to the typical velocity differences between particles at a given distance. This second quantity relates to the particle velocity (first-order) structure function

$$S_1(r) = \left\langle |\boldsymbol{v}_\mathrm{p}^{(1)} - \boldsymbol{v}_\mathrm{p}^{(2)}| \,\middle|\, |\boldsymbol{x}_\mathrm{p}^{(1)} - \boldsymbol{x}_\mathrm{p}^{(2)}| = r \right\rangle \tag{10}$$

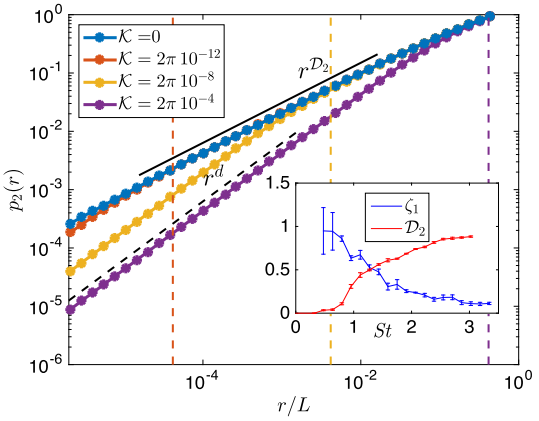

Fig. 3. Cumulative probability $p_2^<(r)$ of inter-particle distances for various diffusivities κ and for $St \approx 2$. One observes at low diffusivities and for $r > \ell_d$ a behavior $\propto (r/L)^{\mathcal{D}_2}$ with $\mathcal{D}_2 \approx 0.7 < d = 1$, followed at small scales by uniform particle distribution where $p_2^<(r) \propto r$. As κ increases, the transition is moved to larger values of r. The vertical dashed represent in each case the estimate $\ell_d \sim \tau_p^{3/2}\kappa^{1/2}$ for this transition. Inset: variations of the correlation dimension $\mathcal{D}_2$ and of the scaling exponent ζ_1 of the first order particle structure function, as a function of the Stokes number St in the case of the random fluid velocity defined by Eqs. (6)–(7).

This is the average of the amplitude of the velocity difference between two particles that are at a given distance r. As the probability of distances, this quantity behaves as a power law $S_1(r) \sim r^{\zeta_1}$ for $r \ll L$ (see e.g. [19]). The exponent ζ_1, shown in the inset of Fig. 3 decreases from 1 at $St = 0$, corresponding to a differentiable particle velocity field, to 0 when $St \to \infty$, which indicates that particle velocity differences become uncorrelated with their distances. Again, when working with the phase–space density one cannot use (10) but relies on

$$S_1(r) = \frac{\left\langle \int \mathrm{d}v \int \mathrm{d}v'\, f(x,v)\, f(x+r,v')\, |v-v'| \right\rangle}{\left\langle \int \mathrm{d}v \int \mathrm{d}v'\, f(x,v)\, f(x+r,v') \right\rangle} \tag{11}$$

As the second-order moment of the coarse-grained density, this quantity will also be used as a physical observable for benchmarking the method.

In the above discussion, we have neglected the effects of diffusion. It is for instance expected to alter clustering properties by blurring the particle distribution at small scales. This is illustrated in Fig. 2 where one can compare the instantaneous phase–space particle positions in the absence of diffusion (Left) and when it is present (Right) at the same time and for the same realization of the fluid velocity. At large scales, identical patterns are present, but diffusion acts at small scale and smoothes out the fine fractal structure of the distribution. One can easily estimate the scales at which this crossover occurs. Diffusion is responsible for a dispersion v_d in velocities that can be obtained by balancing Stokes drag and diffusion in the particle dynamics, namely $v_d^2/\tau_p \approx \kappa$, so that $v_d \sim \tau_p^{1/2}\kappa^{1/2}$. This dispersion in velocity is responsible for a dispersion in positions on scales of the order of $\ell_d = \tau_p\, v_d \sim \tau_p^{3/2}\kappa^{1/2} = St^{3/2}\mathcal{K}^{1/2}L$. Hence, when diffusion is small enough and $\ell_d \ll L$, the spatial distribution of particles is unchanged by diffusion at length scales $r \gg \ell_d$, and the probability that two particles are at a distance less than r behaves as $p_2^<(r) \sim (r/L)^{\mathcal{D}_2}$. For $r \ll \ell_d$, diffusion becomes dominant, the particles distribute in a homogeneous manner and $p_2^<(r) \propto r^d$, with $d = 1$ being the space dimension. By continuity at $r = \ell_d$, we get $p_2^<(r) \sim (\ell_d/L)^{\mathcal{D}_2}(r/\ell_d)$ at small scales.

This picture is confirmed numerically as shown in Fig. 3 which represents the scale-behavior of $p_2^<(r)$ for a fixed Stokes number and various values of the diffusivity κ. One clearly observes the homogeneous distribution $\propto r^d$ at small scales and the fractal scaling $\propto r^{\mathcal{D}_2}$ in an intermediate range. The predicted transition between the two behaviors is indicated by the vertical lines at the diffusive scale ℓ_d. A homogeneous distribution is recovered for $r \lesssim \ell_d/10$.

Velocity statistics are also altered by the presence of diffusion. The structure function $S_1(r)$ is expected to behave as r^{ζ_1} for $\ell_d \ll r \ll L$ and to saturate to a constant value when $r \ll \ell_d$. By continuity, the value of this plateau should be $\sim \ell_d^{\zeta_1} \sim \mathcal{K}^{\zeta_1/2}$. Note finally that the slow convergence $\ell_d/L \propto \sqrt{\mathcal{K}}$ as $\mathcal{K} \to 0$ implies that very small values of the diffusion are needed in order to clearly recover the statistics of diffusive-less particles as an intermediate asymptotics.

3.2. Lattice–particle simulations

We now turn to the application of the lattice–particle method described in Sec. 2 to this one-dimensional situation. We compare the results to Lagrangian simulations where we track the time evolution of N_p particles randomly seeded in space with zero initial velocity. We choose and normalize the initial phase–space density $f(x,v,0)$ to match the Lagrangian settings. The distribution is uniform over the cells, concentrated on a vanishing velocity and the total mass is such that $\sum_{i,j} f(x_i, v_j, t)\, \Delta x\, \Delta v = N_p$. In all simulations, the maximum velocity is set to $V_{\max} = u_{\mathrm{rms}} = 1$ and we have chosen $L = 2\pi$

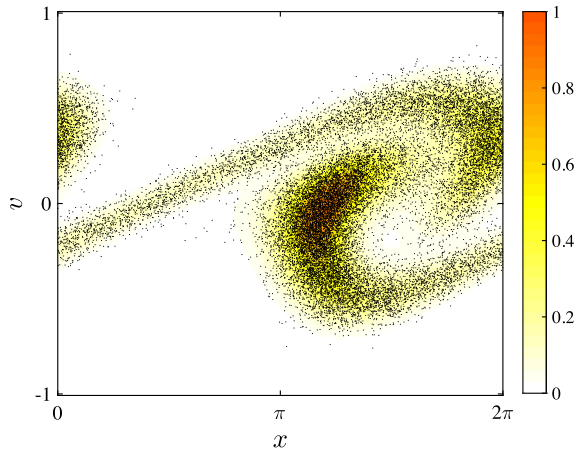

Fig. 4. Position-velocity phase–space positions of Lagrangian particles (black dots) on the top of the field obtained by the lattice–particle method (colored background). The diffusivity is here $\kappa = 10^{-3}$ ($\mathcal{K} \approx 6.28.10^{-3}$) and $St \approx 2$.

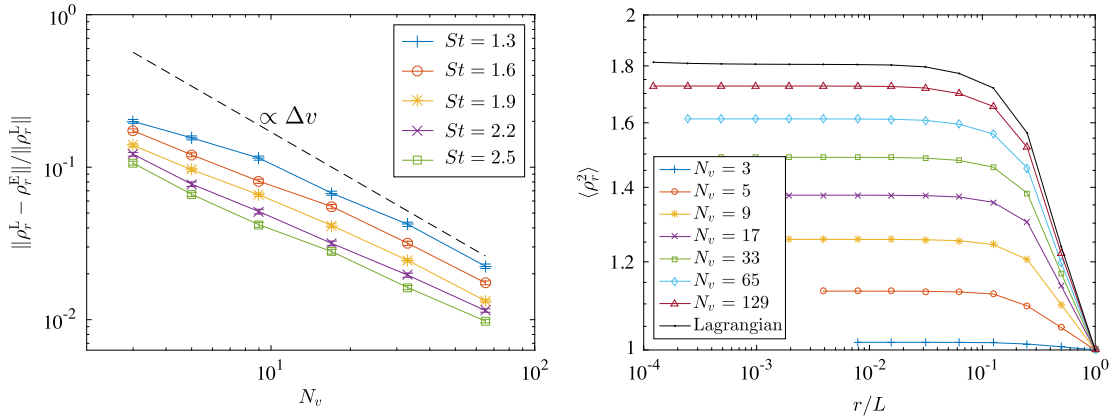

Fig. 5. Left: Relative $\mathcal{L}_2$-error of the lattice–particle method for evaluating the coarse-grained density ρ_r over a scale $r = L/128$ as a function of the number of velocity gridpoints N_v and for various values of the Stokes number, as labeled. Right: Convergence of the second-order moment of the coarse-grained density $\langle \rho_r^2 \rangle$, which is shown as a function of r for $St \approx 1.9$, $\mathcal{K} = \pi 10^{-2}$, and various lattice velocity resolutions N_v, as labeled.

and $\tau_f = 1$. In these units, the time step is kept fixed at $\Delta t = \Delta x/\Delta v = 2^{-6}\pi \approx 0.05$. The number of discrete velocities is of the form $2^n + 1$ and is varied between $N_v = 3$ to 129. The number of spatial collocation points is then given by 2^{n+6} and thus varies between $N_x = 128$ to 8192. Note that, because of the CFL condition (3), this choice restricts the number of discrete velocities that can be used to $N_v < 1 + 128\,St/(2\pi)$.

Fig. 4 represents simultaneously the phase–space distribution of Lagrangian particles and the numerical approximation obtained by the particle-lattice method for $N_v = 129$. Clearly, one observes that the method fairly reproduces the distribution of particles, including the depleted zones, as well as the more concentrated regions. Furthermore, the method is able to catch multivalued particle velocities. We have for instance up to three branches in v for $x \simeq 3\pi/2$. It is important to emphasize that numerical diffusion is of course present, and that it has to be smaller than the physical diffusion κ in order for the approach to be consistent with the Lagrangian dynamics.

To get a more quantitative insight on the convergence of the method, we next compare the coarse-grained densities obtained from the Lagrangian simulation and the lattice–particle approximation of the phase–space density. The first, denoted ρ_r^L is computed by counting the number of particles contained in the different boxes of a tiling of size r. The second is written as ρ_r^E and is obtained by summing over velocities and coarse-graining over a scale r the phase–space density obtained numerically. To confirm the convergence of the method, we measure for a fixed r the behavior of the $\mathcal{L}_2$-norm of the difference between ρ_r^L and ρ_r^E, namely

$$\|\rho_r^L - \rho_r^E\| = \left\langle \left(\rho_r^L(x,t) - \rho_r^E(x,t)\right)^2 \right\rangle^{1/2} \tag{12}$$

where the angular brackets $\langle\cdot\rangle$ encompass a spatial and a time average. Fig. 5 shows the behavior of the relative $\mathcal{L}_2$-error as a function of the number of velocity grid points N_v, for various values of the Stokes number St and for a given scale r. One observes that the error decreases when the resolution increases, giving strong evidence of the convergence of the method.

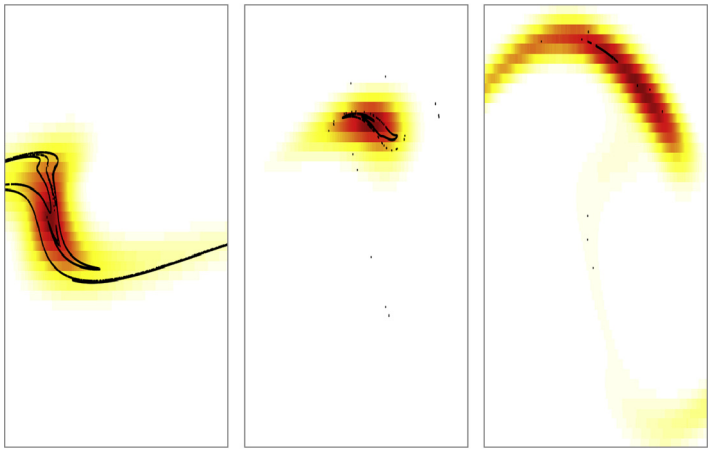

Fig. 6. Three snapshots of the Lagrangian particles (black dots, for $\mathcal{K} = 0$) and of the lattice–particle Eulerian solution (colored background) in the (x, v) plane for different times: at $t < t_\star$ (Left) the solution is well approximated at large scales; at $t = t_\star$ (Center) an order-unity fraction of the mass is concentrated on a scale less than ℓ_d; at $t > t_\star$ (Right), the Eulerian and Lagrangian solutions diverge exponentially fast with differences appearing at the largest scales.

The error is found proportional to the velocity grid spacing Δv, indicating that the method is first order for large values of N_v. The constant is a decreasing function of the Stokes number. This indicates that the method is more accurate for particles with strong inertia. The reason for this trend will be addressed in the sequel.

To assess the ability of the proposed method to reproduce physically relevant quantities, we now compare statistics obtained using the lattice method with those using a Lagrangian approach. We focus on the clustering and velocity difference properties that were introduced and discussed in Section 3.1.

Fig. 5 shows for given values of the Stokes number and of the diffusivity, the second-order moment of the coarse-grained density $\langle(\rho_r^{\mathrm{E}})^2\rangle$ as a function of r and various values of the resolution in velocities, together with the value $\langle(\rho_r^{\mathrm{L}})^2\rangle$ obtained with 10^6 Lagrangian particles. One observes that the curves approach the limiting behavior from below when the number of grid points N_v becomes larger (i.e. when $\Delta v \to 0$). At sufficiently high velocity resolutions, the method is able to capture the large-scale properties of the concentration of the particles. The second-order moment of density then saturates to a value lower than that expected from Lagrangian measurements. The situation is very different at very low resolutions where the data obtained from the lattice–particle method deviates much, even at large scales. This corresponds to the case when the numerical diffusion in velocity is larger than the physical diffusion.

These strong deviations stem from a non-trivial effect of diffusion that lead to finite-scale divergences of the solutions associated with different values of $\mathcal{K}$. In the absence of diffusion, there is a finite probability that an order-one fraction of mass gets concentrated on an arbitrary small subdomain of the position–velocity phase space. This corresponds to a violent fluctuation where the local dimension approaches zero. At the time when this occurs, the mass distribution associated with a finite value of the diffusion will get stacked at a scale ℓ_d. Because of the chaotic nature of the particle dynamics, the two mass distributions, with and without diffusion will experience very different evolutions and diverge exponentially fast. Such a strong clustering event followed by the divergence of the solutions, is shown in Fig. 6. Starting from a correctly reproduced distribution, the major part of non-diffusive Lagrangian particles concentrate into a subgrid region while the Eulerian approximation is stacked at scales of the order of ℓ_d. At a later time, the two distributions diverge and the diffusive particles fill faster larger scales. The probability with which one encounters such a configuration strongly depends on the Stokes number and on the spatial dimension. In the one-dimensional case, such events are rather frequent but become sparser when the Stokes number increases. This is essentially due to the compressibility of the carrier flow. For incompressible fluids in higher dimensions, we expect a negligible contribution from these events.

In addition, we report some results on velocity difference statistics. For that, we have measured the first-order structure function $S_1(r)$ of the particle velocity, using (10) in the Lagrangian case and (11) for solutions obtained with the lattice–particle method. Fig. 7 shows the relative error of $S_1(r)$ for fixed values of the separation $r = 2\pi/2^6 = 2^5\Delta x$, the Stokes number, and the diffusivity, as a function of the velocity resolution. Clearly, when the number of grid points N_v increases, the error decreases, following a law approximatively proportional to the grid spacing Δv. The inset shows the same quantity but, this time, for a fixed resolution ($N_v = 33$) and as a function of the Stokes number. One clearly observes a trend for this error to decrease with St. There are two explanations for this behavior. First, as seen above, there are strong clustering events leading to differences between the Lagrangian and lattice solutions that can persist for a finite time. When the Stokes number increases, such events become less probable. The second explanation relies on the fact that particles with a larger Stokes number experience weaker velocity fluctuations. This implies that for a fixed value of $V_{\max}$, the particle velocity is more likely to be fully resolved at large values of St. As seen in the inset of Fig. 7, the downtrend of the error is compatible with a behavior $\propto St^{-1/2}$. It might thus be proportional to the expected value of the root-mean-squared particle velocity when $St \gg 1$ (see [28]), favoring the second explanation.

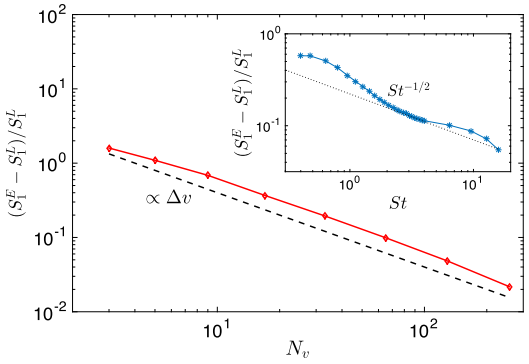

Fig. 7. Relative error between the particle velocity structure function $S_1^E(r)$ obtained from the lattice–particle method and that $S_1^L(r)$ from Lagrangian averages, as a function of the number N_v of velocity grid points. Here, the Stokes number is fixed $St \approx 1.9$ and $\mathcal{K} = 2\pi 10^{-3}$. Inset: same quantity but for $N_v = 33$ and as a function of the Stokes number St.

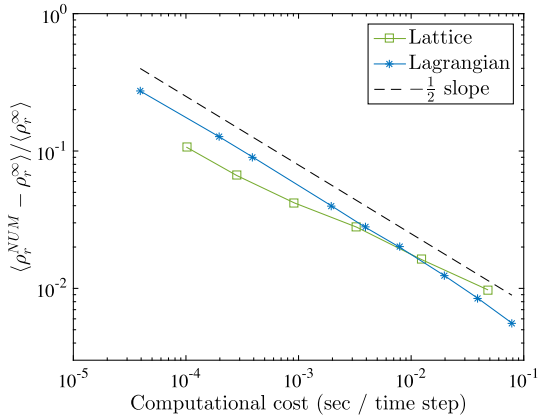

Fig. 8. Relative $\mathcal{L}_2$ errors on the coarse-grained density fields obtained with either Lagrangian or lattice simulations, plotted here as a function of the computational cost (same parameters as in Fig. 5 for $St = 2.5$). The various simulations were done with a fixed time stepping $\Delta t = 5 \times 10^{-2}$; the lattice case spans $N_v = 3$ to 65, while the Lagrangian simulations correspond to a number of particles N_p varying from 10^3 to 2×10^6. The symbol in the y-axis label stands for either Lagrangian of Eulerian simulations.

To close this section on one-dimensional benchmarks of the lattice–particle method, we briefly assess the numerical cost of the method. The computational cost per time step for both Lagrangian and Lattice simulations are compared for a fixed resolution and coarse-graining scale. A reference coarse-grained density field ρ_r^∞ from the Lagrangian method using a large number of particles ($N_\mathrm{p} = 10^7$) is compared to the ones ρ_r^NUM obtained either from the Lattice or the Lagrangian simulations varying the resolution (number of velocities N_v for the lattice method or the number N_p of Lagrangian particles). All the density fields are coarse-grained at the same scale $r = L/128$ as in Fig. 5. Fig. 8 shows the relative error as a function of the computational cost. All the simulations were done using the same quadri-core CPU with shared memory. We expect the costs to have the same tendencies when using distributed memory machines, as the communication should not vary much from one method to the other. For the Lagrangian simulations, the error is essentially given by finite number effects that affect the resolution of the particle density field. It is thus related to the statistical convergence of the average and behaves as $N_\mathrm{p}^{-1/2}$. As the computational cost is proportional to N_p, this explains the 1/2-scaling observed in Fig. 8. For the lattice simulations the cost is proportional to N_v^2, since increasing N_v with constant time step implies increasing N_x by the same factor. It appears that the Lattice method is more computationally efficient down to a given error. A few number of discrete velocities reproduces indeed better the reference density field than Lagrangian simulations with too few particles. The crossover observed in Fig. 8 is due to the scaling of the error with respect to N_v that is slightly slower than linear, as shown in Fig. 5. Note that if the advection term in equation (2) is treated with a higher order scheme, the error as a function of N_v will decrease faster than linearly, and the Lattice method will be computationally advantageous if lesser errors are targeted. Finally, let us stress that the comparison is here performed for the simple case of non-interacting particles. In some situations involving long-range interactions (such as gravitational or electrical forces), Lagrangian methods might require $\mathrm{O}(N_\mathrm{p}^2)$ operations and become much less efficient that the lattice method, which will then still have a cost $\mathrm{O}(N_x \times N_v)$.

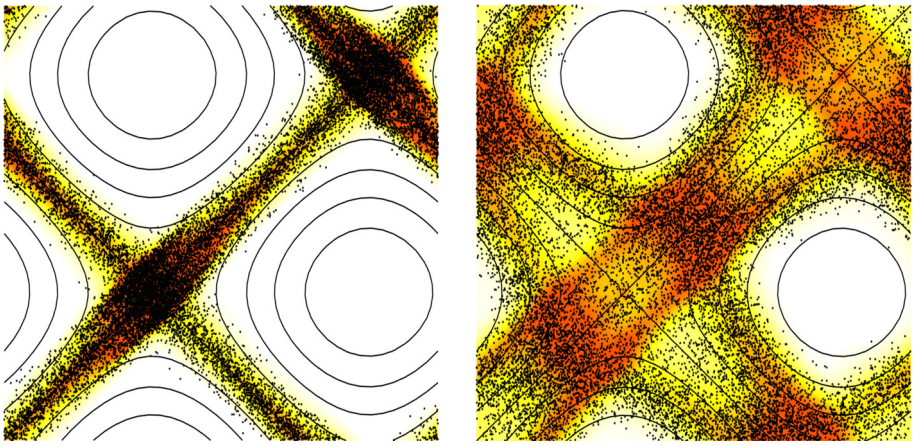

Fig. 9. Particles stationary distribution inside a tilted cellular flow along with the density field from the lattice method. The value of the diffusivity is $\mathcal{K} = 8\pi \times 10^{-3}$. Left: $St = 1/(2\pi)$. Right: $St = 1/\pi$. These simulations were performed on a lattice with 1024^2 spatial gridpoints associated with 19^2 discrete velocities. The distributions have been here spatially shifted in order to avoid having the concentration point $(0, 0)$ at the origin.

4. Application to incompressible two-dimensional flows

We extend in this section the lattice–particle method to two-dimensional flows. For the particle acceleration, we again make use of a flux-limiter scheme.

4.1. Cellular flow

We first consider a fluid flow that is a stationary solution to the incompressible Euler equations (and to the forced Navier–Stokes equations). It consists of a cellular flow field, a model that have often been used to investigate mixing properties, as well as the settling of heavy inertial particles (see, e.g., [33,34]). The velocity field is the orthogonal gradient of the L-periodic bimodal stream function $\psi(x, y) = U \sin(\pi(x+y)/L) \sin(\pi(x-y)/L)$ (the typical velocity strength is here denoted by U). The cellular flow has been here tilted by an angle $\pi/4$ in order to avoid any alignment of the separatrices between cells with the lattice that leads to spurious anisotropic effects.

Fig. 9 shows two snapshots for two different values of $St = \tau_p U/L$ of the stationary particle distribution (black dots), together with the density field evolved by the lattice–particle dynamics. For the smallest Stokes number (Left panel), one observes that the particle distribution is concentrated along the separatrices between the different cells. One also observes that it develops entangled structures in the vicinity of the hyperbolic stagnation points of the flow. These loops, which are aligned with the stable direction, corresponds to oscillations in the particle dynamics that occurs when their inertia makes them cross the unstable manifold with a too large velocity. At larger St, the particle distribution is somewhat broader but is this time centered on specific trajectories that do not perform the aforementioned oscillation but rather cross ballistically the heteroclinic separatrices. In both cases the particle distribution contains regions where trajectories are clearly crossing each other. The lattice method reproduces fairly well this complex dynamics. Note that any traditional Eulerian–Eulerian method introducing a particle velocity field will not be able to reproduce such effects.

4.2. Heavy particles in 2D turbulence

We next turn to the application of the method in non-stationary fluid flows that are solutions to the forced two-dimensional incompressible Navier–Stokes equations

$$\partial_t \boldsymbol{u} + \boldsymbol{u} \cdot \nabla \boldsymbol{u} = -\frac{1}{\rho_f} \nabla p + \nu \nabla^2 \boldsymbol{u} - \alpha \boldsymbol{u} + \boldsymbol{f}, \quad \nabla \cdot \boldsymbol{u} = 0 \tag{13}$$

The linear damping term involving the coefficient α originates from Ekman friction (in geophysical flows), Rayleigh friction (in stratified fluids) or the friction induced by the surrounding air in soap-film experiment. The flow is maintained in a statistical steady state by the forcing $\boldsymbol{f}$ that is assumed to be concentrated over a specific scale ℓ_f. The fluid velocity field $\boldsymbol{u}$ is computed numerically using a pseudo-spectral, fully de-aliased GPU solver for the vorticity-streamfunction formulation of the Navier–Stokes equation (13).

Kinetic energy is known to undergo in two dimensions an *inverse cascade* [35] with a rate ε toward the large scales $\ell \gg \ell_f$ where it is dissipated by the linear damping. For $k \ll k_f \propto \ell_f^{-1}$, this promotes a $k^{-5/3}$ Kolmogorov law, as in the three-dimensional direct cascade. The particle distribution at such scales is difficult to characterize because of the scale-invariance of the velocity field. Neither the moments of the coarse-grained density nor the particle velocity structure functions display any scaling behavior. What has been nevertheless observed numerically in [36] is that the particle spatial distribution is

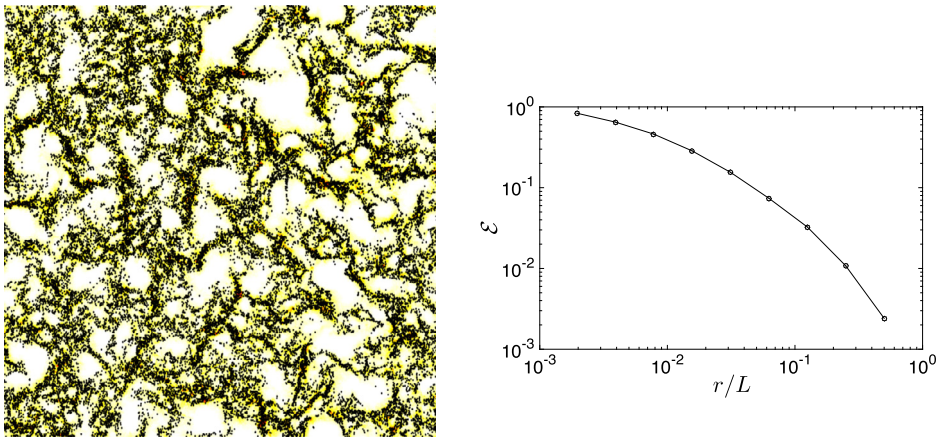

Fig. 10. Left: Snapshot of the position of Lagrangian particles (black dots), together with the density field obtained from the lattice method (colored background, from white: low densities to red: high densities) for $St \approx 0.1$ in the inverse energy cascade. The fluid flow was integrated using a resolution of 2048^2 and lattice simulations were performed with 512^2 spatial grid points associated with 9^2 discrete velocities. Right: Relative error $\mathcal{E}$ of the second-order moment of the coarse-grained density ρ_r as a function of r for $St = 0.5$. The lattice–particle method was here used with 512^2 position grid points and 9^2 velocity grid points.

dominated by the presence of voids whose sizes obey a universal scaling law. It is argued in [37] that such voids are related to the excited regions of the flow and that particles tend to follow the calm regions where the zeros of the fluid acceleration are more probable.

We have tested the proposed lattice method in a two-dimensional turbulent flow in the inverse kinetic energy cascade regime. The stochastic forcing is acting at small scales ($400 \leq |\boldsymbol{k}| \leq 405$) and we made use of hyper-viscosity (here eighth power of the Laplacian) in order to truncate any possible direct enstrophy cascade. The kinetic energy accumulated at large scales is removed using a linear friction in the Navier–Stokes equation (13). The particle Stokes number is defined as $St = \tau_p/\tau_L$ using the large-eddy turnover time $\tau_L = L/u_{\rm rms}$ since small-scale statistics are dominated by forcing and are thus irrelevant. The flow is integrated with a resolution of 2048^2 gridpoints while the lattice–particle method is applied for $St \approx 0.1$ on a coarser grid with 512^2 points.

Fig. 10 (Left) shows that the lattice–particle method is able to reproduce the main qualitative features of the particle spatial distribution at scales within the inertial range of the inverse energy cascade. Focusing again on the second-order statistics of the particle mass distribution, we have measured the average with respect to r of the error made on the density moment $\langle \rho_r^2 \rangle$ defined as

$$\mathcal{E} = \overline{\langle (\rho_r^{\rm E})^2 \rangle - \langle (\rho_r^{\rm L})^2 \rangle} \,/\, \overline{\langle (\rho_r^{\rm L})^2 \rangle} \tag{14}$$

where

$$\overline{f(r)} = \frac{1}{L^2} \int_0^L |f(r)|\, r \, {\rm d}r \tag{15}$$

Fig. 10 (Right) represents this relative error $\mathcal{E}$ as a function of the coarse-graining scale r. The Lagrangian integration was performed with 2×10^7 particles (with no physical diffusion) and the lattice method on a 512^2 spatial grid with $N_v^2 = 9^2$ discrete values of the particle velocity. One clearly observes that the error decreases at the largest scales of the flow.

5. Conclusions

We have presented a new Eulerian numerical method to simulate the dynamics of inertial particles suspended in unsteady flow. This lattice–particle method is based on the discretization in the position–velocity phase space of the evolution equation for the particle distribution. The spatial grid is chosen such that particles with a given discrete velocity hop by an integer number of gridpoints during one time step, an idea close to that used in lattice–Boltzmann schemes. We have shown that the method reproduces the correct dynamical and statistical properties of the particles, even with a reasonably small amount of velocity gridpoints. Some deviations from Lagrangian measurements are nevertheless observed at small scales in one dimension. We obtained evidence that they are due to numerical diffusivity acting in the space of velocities and are more important in one dimension at small Stokes numbers than otherwise. The proposed method is anyway intended to describe large scales where such deviations disappear. It might hence be a suitable candidate for developing large-eddy models for particle dynamics. Indeed, as equation (2) is linear in f, some techniques of subgrid modeling used in scalar turbulent transport (see [38] for example) could be adapted.

Our approach consists in always imposing the same mesh for particle velocities, independently of the spatial position and of the local value of the fluid velocity. This is particularly well-adapted for particles with a large Stokes number. Their velocity experiences small fluctuations and is generally poorly connected to that of the fluid. In addition, the method is accurate at the largest scales and can hence catch the structures appearing in the spatial and velocity distributions of large-Stokes-number particles. Such considerations indicate that the proposed lattice–particle method is suitable for simulating particles with a sufficiently strong inertia. Conversely, particles with a weak inertia develop fine-scale structures in their distribution. They result from tiny departures of their velocity from that of the fluid. Our method, applied with a fixed velocity resolution, might not be able to catch such deviations. However, a more suitable idea for this case is to use a variation of our approach where, instead of a full resolution of the particle velocity, one considers its difference with that of the fluid. This would of course require changing scheme for integrating advection but should in principle not lead to any major difficulty.

Acknowledgements

This study benefited from fruitful discussions with M. Gorokhovski, H. Homann, S. Musacchio. The research leading to these results has received funding from the Agence Nationale de la Recherche (Programme Blanc ANR-12-BS09-011-04) and from the European Research Council under the European Community's Seventh Framework Programme (FP7/2007–2013 Grant Agreement No. 240579). Numerical simulations were performed on the Mésocentre de calcul SIGAMM.

References

[1] F. Toschi, E. Bodenschatz, Lagrangian properties of particles in turbulence, Annu. Rev. Fluid Mech. 41 (2009) 375–404.
[2] S. Balachandar, J.K. Eaton, Turbulent dispersed multiphase flow, Annu. Rev. Fluid Mech. 42 (2010) 111–133.
[3] Q. Wang, K.D. Squires, Large eddy simulation of particle-laden turbulent channel flow, Phys. Fluids 8 (5) (1996) 1207–1223.
[4] B. Shotorban, F. Mashayek, A stochastic model for particle motion in large-eddy simulation, J. Turbul. 7 (18) (2006), http://dx.doi.org/10.1080/14685240600595685.
[5] J. Pozorski, S.V. Apte, Filtered particle tracking in isotropic turbulence and stochastic modeling of subgrid-scale dispersion, Int. J. Multiph. Flow 35 (2) (2009) 118–128.
[6] S.-I. Shima, K. Kusano, A. Kawano, T. Sugiyama, S. Kawahara, The super-droplet method for the numerical simulation of clouds and precipitation: a particle-based and probabilistic microphysics model coupled with a non-hydrostatic model, Q. J. R. Meteorol. Soc. 135 (642) (2009) 1307–1320.
[7] H. Rein, G. Lesur, Z.M. Leinhardt, The validity of the super-particle approximation during planetesimal formation, Astron. Astrophys. 511 (2010) A69.
[8] L.M. Portela, R.V.A. Oliemans, Possibilities and limitations of computer simulations of industrial turbulent dispersed multiphase flows, Flow Turbul. Combust. 77 (1–4) (2006) 381–403.
[9] R.O. Fox, Large-eddy-simulation tools for multiphase flows, Annu. Rev. Fluid Mech. 44 (2012) 47–76.
[10] S. Morioka, T. Nakajima, Modeling of gas and solid particles 2-phase flow and application to fluidized-bed, J. Méc. Théor. Appl. 6 (1) (1987) 77–88.
[11] M. Reeks, On a kinetic equation for the transport of particles in turbulent flows, Phys. Fluids A 3 (3) (1991) 446–456.
[12] P. Fede, V. Sofonea, R. Fournier, S. Blanco, O. Simonin, G. Lepoutère, V. Ambruş, Lattice Boltzmann model for predicting the deposition of inertial particles transported by a turbulent flow, Int. J. Multiph. Flow 76 (2015) 187–197.
[13] J.-A. Carrillo, T. Goudon, P. Lafitte, Simulation of fluid and particles flows: asymptotic preserving schemes for bubbling and flowing regimes, J. Comput. Phys. 227 (16) (2008) 7929–7951.
[14] M.R. Maxey, The gravitational settling of aerosol particles in homogeneous turbulence and random flow fields, J. Fluid Mech. 174 (1987) 441–465.
[15] B. Shotorban, S. Balachandar, A Eulerian model for large-eddy simulation of concentration of particles with small Stokes numbers, Phys. Fluids 19 (11) (2007) 118107.
[16] X.-Q. Chen, Heavy particle dispersion in inhomogeneous, anisotropic, turbulent flows, Int. J. Multiph. Flow 26 (4) (2000) 635–661.
[17] G. Falkovich, A. Fouxon, M. Stepanov, Acceleration of rain initiation by cloud turbulence, Nature 419 (6903) (2002) 151–154.
[18] M. Wilkinson, B. Mehlig, Caustics in turbulent aerosols, Europhys. Lett. 71 (2) (2005) 186.
[19] J. Bec, A. Celani, M. Cencini, S. Musacchio, Clustering and collisions of heavy particles in random smooth flows, Phys. Fluids 17 (7) (2005) 073301.
[20] P. Fevrier, O. Simonin, K.D. Squires, Partitioning of particle velocities in gas–solid turbulent flows into a continuous field and a spatially uncorrelated random distribution: theoretical formalism and numerical study, J. Fluid Mech. 533 (2005) 1–46.
[21] O. Desjardins, R.O. Fox, P. Villedieu, A quadrature-based moment method for dilute fluid-particle flows, J. Comput. Phys. 227 (4) (2008) 2514–2539.
[22] H. Liu, Z. Wang, R.O. Fox, A level set approach for dilute non-collisional fluid-particle flows, J. Comput. Phys. 230 (4) (2011) 920–936.
[23] S. Chen, G.D. Doolen, Lattice Boltzmann method for fluid flows, Annu. Rev. Fluid Mech. 30 (1) (1998) 329–364.
[24] R.J. LeVeque, Finite Volume Methods for Hyperbolic Problems, Cambridge Univ. Press, 2002.
[25] S. Succi, The Lattice Boltzmann Equation for Fluid Dynamics and Beyond, Oxford University Press, USA, 2001.
[26] W. Hundsdorfer, B. Koren, J. Verwer, et al., A positive finite-difference advection scheme, J. Comput. Phys. 117 (1) (1995) 35–46.
[27] B. Koren, A robust upwind discretization method for advection, diffusion and source terms, Centrum voor Wiskunde en Informatica Amsterdam, 1993.
[28] J. Abrahamson, Collision rates of small particles in a vigorously turbulent fluid, Chem. Eng. Sci. 30 (11) (1975) 1371–1379.
[29] H. Hentschel, I. Procaccia, The infinite number of generalized dimensions of fractals and strange attractors, Physica D 8 (3) (1983) 435–444.
[30] J. Bec, Fractal clustering of inertial particles in random flows, Phys. Fluids 15 (11) (2003) L81–L84.
[31] M. Wilkinson, B. Mehlig, Path coalescence transition and its applications, Phys. Rev. E 68 (4) (2003) 040101.
[32] S. Sundaram, L. Collins, Collision statistics in an isotropic particle-laden turbulent suspension. Part 1. Direct numerical simulations, J. Fluid Mech. 335 (1997) 75–109.
[33] M.R. Maxey, S. Corrsin, Gravitational settling of aerosol particles in randomly oriented cellular flow fields, J. Atmos. Sci. 43 (11) (1986) 1112–1134, http://dx.doi.org/10.1175/1520-0469(1986)043<1112:GSOAPI>2.0.CO;2.
[34] L. Bergougnoux, G. Bouchet, D. Lopez, E. Guazzelli, The motion of solid spherical particles falling in a cellular flow field at low Stokes number, Phys. Fluids 26 (9) (2014) 093302.
[35] G. Boffetta, R.E. Ecke, Two-dimensional turbulence, Annu. Rev. Fluid Mech. 44 (2012) 427–451.
[36] G. Boffetta, F. De Lillo, A. Gamba, Large scale inhomogeneity of inertial particles in turbulent flows, Phys. Fluids 16 (4) (2004) L20–L23.
[37] L. Chen, S. Goto, J. Vassilicos, Turbulent clustering of stagnation points and inertial particles, J. Fluid Mech. 553 (2006) 143–154.
[38] S.S. Girimaji, Y. Zhou, Analysis and modeling of subgrid scalar mixing using numerical data, Phys. Fluids 8 (5) (1996) 1224–1236.